Effect of Fabrication Parameters on Three-Dimensional Nanostructures of Bulk Heterojunctions Imaged by High-Resolution Scanning ToF-SIMS

Bang-Ying Yu,[†] Wei-Chun Lin,[†] Wei-Ben Wang,[§] Shin-ichi Iida,[∥] Sun-Zen Chen,[⊥] Chia-Yi Liu,[†] Che-Hung Kuo,[‡] Szu-Hsian Lee,[‡] Wei-Lun Kao,[‡] Guo-Ji Yen,[‡] Yun-Wen You,[†] Chi-Ping Liu,[†] Jwo-Huei Jou,[§] and Jing-Jong Shyue[†,‡,*]

[†]Research Center for Applied Sciences, Academia Sinica, Taipei 115, Taiwan, [‡]Department of Materials Science and Engineering, National Taiwan University, Taipei 106, Taiwan, [§]Department of Materials Science and Engineering, National Tsing Hua University, Hsin-Chu 300, Taiwan, [∥]Analysis Laboratory, ULVAC-PHI, Inc., Chigasaki 253-8522, Japan, and [⊥]Center for Nanotechnology, Materials Science, and Microsystems, National Tsing Hua University, Hsin-Chu 300, Taiwan

ABSTRACT Solution processable fullerene and copolymer bulk heterojunctions are widely used as the active layers of solar cells. In this work, scanning time-of-flight secondary ion mass spectrometry (ToF-SIMS) is used to examine the distribution of [6,6]phenyl-C61-butyric acid methyl ester (PCBM) and regio-regular poly(3-hexylthiophene) (*rr*P3HT) that forms the bulk heterojunction. The planar phase separation of P3HT:PCBM is observed by ToF-SIMS imaging. The depth profile of the fragment distribution that reflects the molecular distribution is achieved by low energy Cs^+ ion sputtering. The depth profile clearly shows a vertical phase separation of P3HT:PCBM before annealing, and hence, the inverted device architecture is beneficial. After annealing, the phase segregation is suppressed, and the device efficiency is dramatically enhanced with a normal device structure. The 3D image is obtained by stacking the 2D ToF-SIMS images acquired at different sputtering times, and 50 nm features are clearly differentiated. The whole imaging process requires less than 2 h, making it both rapid and versatile.

KEYWORDS: secondary ion mass spectrometry · X-ray photoelectron spectrometry · nanostructure · bulk heterojunction · solar cell

Nanostructured polymer solar cells are promising sources of renewable energy due to their simple fabrication process and relatively low cost compared with silicon-based solar cells. One of the most important components of the polymer solar cell is the bulk heterojunction,[1] which consists of a mixture of polymer/organic n- and p-type semiconductors. The most common and well-characterized polymer photovoltaic cells are based on regio-regular poly(3-hexylthiophene) (P3HT, as the p-type material) and [6,6]-phenyl-C61-butyric acid methyl ester (PCBM, as the n-type material).[1,2] The bicontinuous network is formed spontaneously in the mixture and ensures a large interfacial contact area between these two components while providing an adequate path for charge carriers, thereby significantly enhancing the charge separation capability. Due to the limited exciton diffusion length, typically in the 5−15 nm range,[3] the electron acceptor must be intermixed with the polymers on the nanometer scale to obtain a high charge separation yield.[4] Therefore, the control of the nanostructure is crucial to the development of polymer solar cells.[5−7]

In the polymer bulk heterojunction, the heterointerface and percolation network are highly sensitive to process conditions[8−10] and post-treatments.[10,11] In order to understand the relationship between the fabrication parameters, the morphology, and the device efficiency, techniques such as scanning probe microscopy (SPM)[12−16] and variable-angle spectroscopic ellipsometry (VASE)[17] are used to analyze the surface morphology and the vertical distribution, respectively. On the basis of a lift-off sample preparation and X-ray photoelectron spectroscopy (XPS), the vertical phase separation in bulk heterojunctions has also been reported.[13] However, these well-established techniques cannot provide a clear 3D volume structure at the nanometer scale.

Recently, significant efforts have been directed at analyzing the 3D nanostructure of bulk heterojunctions. On the basis of transmission electron microscopy (TEM), electron tomography (ET) is used to examine the 3D structures inside bulk heterojunction specimens.[6,18,19] However, TEM depends on electron scattering to generate contrast, and therefore, amorphous

*Address correspondence to shyue@gate.sinica.edu.tw.

Received for review October 20, 2009 and accepted January 15, 2010.

Published online January 25, 2010.
10.1021/nn9014449

organic materials with similar scattering factors show weak contrast without defocus. The quality of the image depends on the transfer function of the microscope, and moreover, the contrast of the resulting image is more related to the difference in crystallinity rather than on the distribution of the molecules. In addition, inelastic electron scattering and dynamic scattering in thick samples generate diffused backgrounds that further diminish the contrast. As a result, the thickness of samples for TEM study is limited to ~100 nm, and this restriction prevents the analysis of structures in their original states. In addition, due to the limited tilt angle (usually ±70°), it is not possible to obtain complete information for 3D reconstructions, and the missing wedge/pyramid of data in Fourier space can cause artifacts.[20] These issues make electron tomography difficult to master and to apply to multilayered organic electronic devices, particularly in the context of amorphous organic materials.

Another emerging technique for obtaining the 3D distribution of organic molecules is scanning time-of-flight secondary ion mass spectrometry (ToF-SIMS) with cluster ion sputtering.[21−25] Although cluster ion sputtering significantly damages the outermost surface of inorganic materials,[26] it was found to cause insignificant damage to organic surfaces[27,28] because of the shallower damage range[29] and enhanced sputtering rate.[30] As a result, the damage to the specimen can be removed nearly as fast as it is created during the sputtering. Although the sputtering can alter the surface morphology and deposit carbon in the remaining surface, the SIMS patterns before and after cluster ion sputtering remain the same, and the preservation of *m/z* near 1000 is reported.[31] Such evidence indicates that the cluster ion sputtering does not significantly alter the molecular structure and its distribution in the remaining surface. Although the morphology of newly exposed surface can be altered significantly during the removal of the surface layer, enough integrity is maintained so that information beneath the outermost surface can be acquired. Recently, *in situ* cluster ion sputtering in XPS and ToF-SIMS has been used to study the depth distribution of molecules in organic LEDs to examine the microstructures[31] and degradation mechanisms.[32] In combination with the high lateral resolution of SPM, cluster ion slicing imaging was also demonstrated for analyzing the 3D nanostructures of bulk heterojunctions.[33] These techniques only require the specimen to be compatible with ultrahigh vacuum, and organic thin-film devices usually fulfill this requirement. Therefore, organic electronic devices can be analyzed without prior sample preparation. In other words, cluster ion beam-based analytical techniques are now accepted methods, and they provide invaluable structural information about organic electronics.

In this work, scanning ToF-SIMS with *in situ* ion sputtering was used to study bulk heterojunction materials prepared with different fabrication parameters. Using a newly constructed Bi_3^{2+} focused primary ion pulse, a high spatial resolution ToF-SIMS image is obtained that reveals ~50 nm phase separation in organic electronics. Although C implantation associated with C_{60}^+ ion sputtering can interfere with the mapping of the PCBM distribution, a carefully tuned Cs^+ ion beam can be used to sputter the materials away with no significant alteration to the molecular structure in the remaining surface, hence enough integrity is maintained in the newly exposed surface for analysis. By stacking the images acquired at different sputtering times, the 3D volume structure is obtained. It is found that the lateral structure did not change significantly with heat treatment. However, the difference in the vertical phase segregation is clearly observed and is the key to the differences in the performance of devices fabricated with different parameters and device architectures.

RESULTS AND DISCUSSION

By scanning the newly constructed field emission Bi^{x+} ion source over the sample, the distribution of materials can be imaged. However, in order to achieve sufficient lateral resolution (fine probe size) for imaging organic electronics, the current of the primary ion must be rather small (2 fA). As a consequence, the intensity of secondary particles is very weak. In addition, >90% of the secondary particles emitted from the specimen after primary ion bombardment are neutral. Therefore, less than 5% of the emitted particles contribute to the image without a synchronously operated post laser-ionization pulse (as in time-of-flight secondary neutral mass spectrometry, ToF-SNMS), making the signal-to-noise ratio of the resulting image rather poor. In order to improve the contrast, a low-pass filter in Fourier space is used to process the image. In order to confirm that the filter does not enhance noise and that it reveals accurate information, images of different scan sizes are compared.

Figure 1 shows the intensity mapping of C_2 and S fragments with 10 and 5 μm fields-of-view. Because only P3HT contains S atoms, the intensity of the S fragments is directly proportional to the distribution of the P3HT. For PCBM, C_n fragments can be used because C_{60} typically forms C_n fragments while alkyl chains in P3HT mainly generate C_nH_m fragments. It is clear that similar ~50 nm features are observed regardless of the scan size. In addition, these images are similar to surface images previously reported using other techniques.[11,12,33,34] Therefore, it can be concluded that the imaging conditions are adequate for imaging organic electronics with features of ~50 nm. However, unlike TEM, which has a resolution around 1 nm and is controlled by the aberration of the lens, the resolution of ToF-SIMS is limited by the spot size of the primary ion, and hence, the resolution is not as good as with TEM. Therefore, 5−15 nm fibrous structures observable

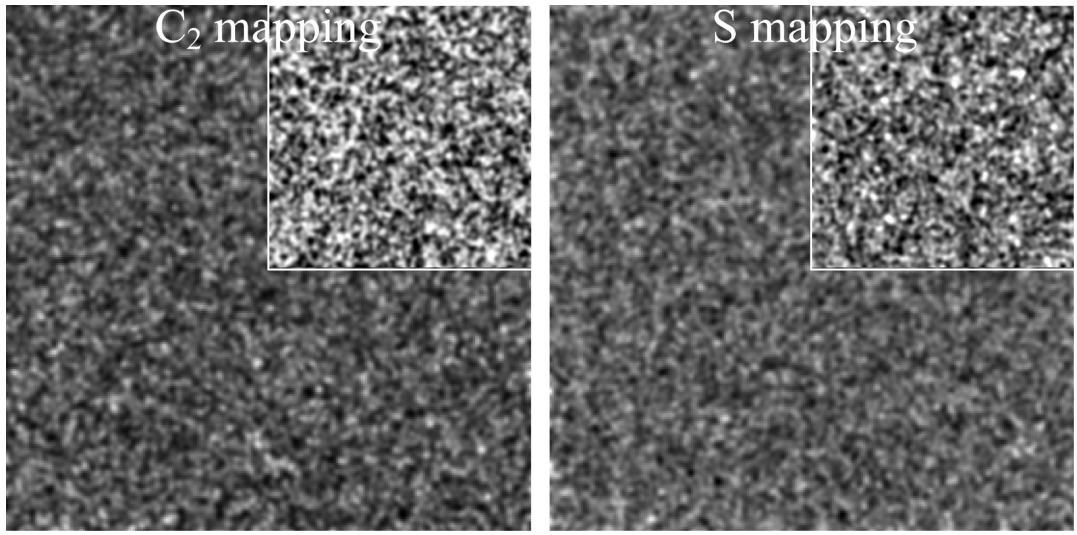

Figure 1. ToF-SIMS intensity mapping of C_2 and S fragments. The main image size is 10 μm × 10 μm, and the inset image size is 5 μm × 5 μm.

by TEM[7] cannot be observed here. Nevertheless, while TEM provides contrast through the difference in scattering factors, which relates indirectly to the distribution of chemical species, the contrast in ToF-SIMS image reveals the number of molecules on the surface. Therefore, ToF-SIMS imaging has the advantages that the difference in chemical structure of specimens can be imaged directly.

In order to study the structure below the surface, *in situ* ion sputtering is typically used. It has been shown that C_{60}^+ cluster ion beams do not alter the remaining P3HT:PCBM surface significantly,[28,33] so C_{60}^+ sputtering is ideal for profiling organic P3HT:PCBM blends. However, it is known that C_{60}^+ can deposit amorphous carbon in the surface,[27,28] hence the observed C concentration is often higher than expected. Figure 2a shows the XPS depth profiling using C_{60}^+ sputtering, and the observed 97% C concentration is higher than the expected 95% for P3HT:PCBM blend. Since this implanted carbon also yields C_n fragments upon primary ion bombardment, C_{60}^+ sputtering can interfere with the analysis of PCBM distribution because the C_2 fragment is used to identify the concentration of PCBM and it is not possible to differentiate the PCBM from deposited C. Instead of a C_{60}^+ ion beam, this work uses Cs^+ ion sputtering for the ToF-SIMS depth profiling. It is known that single atomic ion species such as Ar^+ can alter the chemical structure even at low energy, and unreliable results can be generated.[27,35] Therefore, the possibility of Cs^+ ion-induced chemical transformations in the remaining surface needs to be ruled out. The C_{60}^+ ion sputtering in XPS depth profiling is an accepted method because it is known to preserve the chemical information of the sample.[28] A comparison of this method (Figure 2a) with the ToF-SIMS depth profile from Cs^+ ion sputtering (Figure 2b) reveals few differences. Because the specimen was analyzed without prior sample preparation and cleaning processes, the apparent S/C ratio is rather high due to surface contamination. The SO_3-related signal indicates that the bottom PEDOT:PSS interface was reached, and the sputtering rate can be calibrated to 0.63 nm/min and 0.1 nm/s for XPS/C_{60}^+ and ToF-SIMS/Cs^+, respectively. In the bulk of the polymer blend, both profiles show high S concentrations (characteristic of P3HT) in the top 20% (~30 nm from the outermost surface) of the film, and this concentration slowly decreases to a constant concentration of 45% (~68 nm in depth). The similarities in

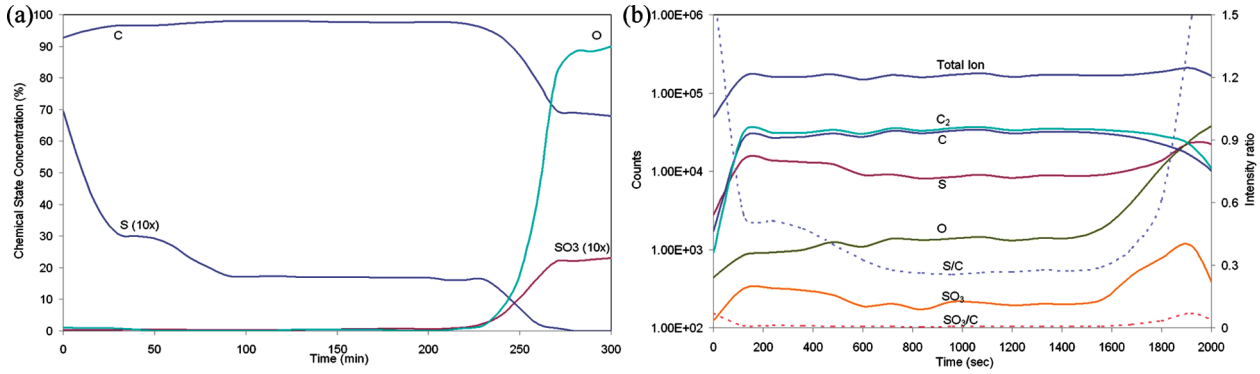

Figure 2. (a) C_{60}^+/XPS and (b) Cs^+/ToF-SIMS depth profiles of pristine specimens. The broken lines indicate the intensity ratios.

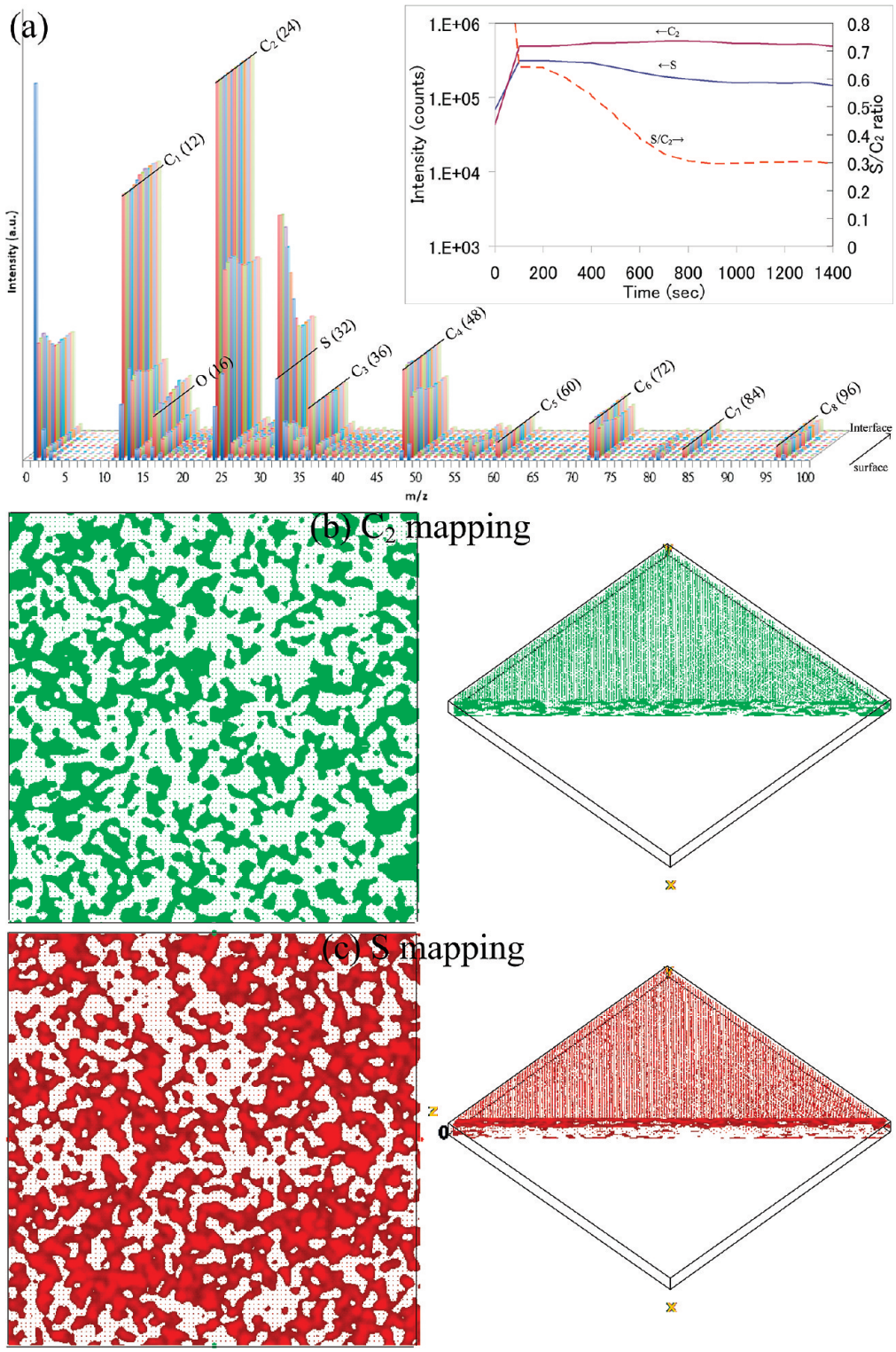

Figure 3. (a) ToF-SIMS spectra normalized to the intensity of C_2; the inset shows the intensity depth profile, and the broken line indicates the intensity ratio; (b,c) intensity isosurface of the outermost surface, and reconstructed cross-sectional structure for the pristine P3HT:PCBM blend. The image size is 3.5 μm × 3.5 μm × 150 nm.

the depth profiles acquired with independent techniques confirm that the conditions of Cs^+ sputtering used in this work preserved the chemical structure in the remaining surface and can be used to generate reliable depth profiles. This success in Cs^+ profiling could be attributed to the implantation of Cs enhanced ionization, hence the damage in the newly exposed surface is masked.

By using *in situ* Cs^+ ion sputtering for ToF-SIMS, surface structures and reconstructed cross-sectional structures for pristine and annealed specimens can be obtained (Figure 3 and Figure 4, respectively). The 3D

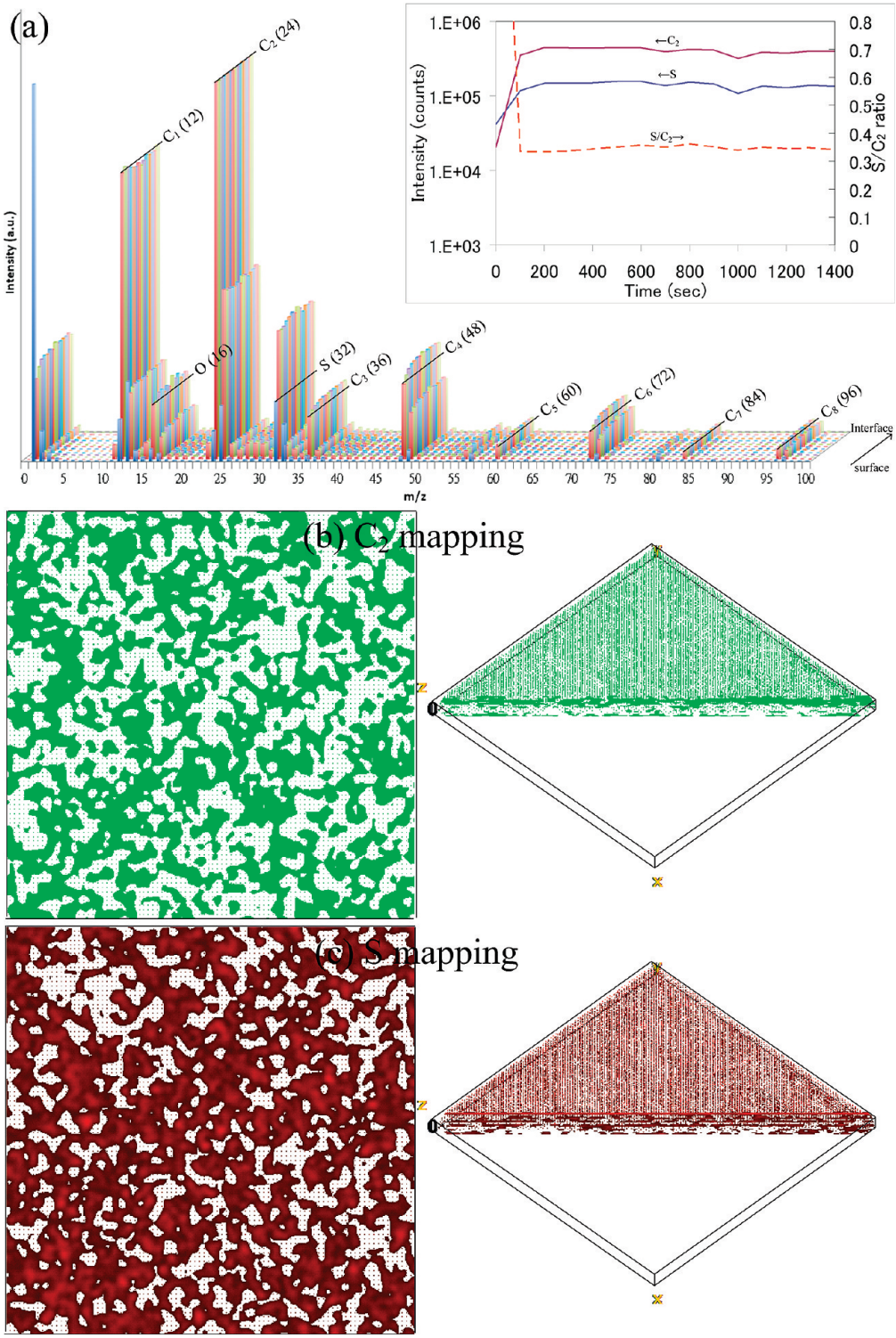

Figure 4. (a) ToF-SIMS spectra normalized to the intensity of C_2; the inset shows the intensity depth profile, and the broken line indicates the intensity ratio; (b,c) intensity isosurface of the outermost surface, and the reconstructed cross-sectional structure for the annealed P3HT:PCBM blend. The image size is 3.5 μm × 3.5 μm × 150 nm.

structure is reconstructed by stacking 15 slices with 100 s sputtering intervals. The animated cross-sectional structure at different slices is presented in the Supporting Information. Considering the sputtering rate determined from Figure 2b, the vertical distance between the slices is around 10 nm. The sputtering rate (and hence the slice thickness) is easily controlled by altering either the rastering size or the current of the sputtering ion beam. In other words, the vertical resolution of the reconstructed 3D image can be adjusted easily.

The reconstructed 3D nanostructures inside the bulk heterojunctions that were acquired using scan-

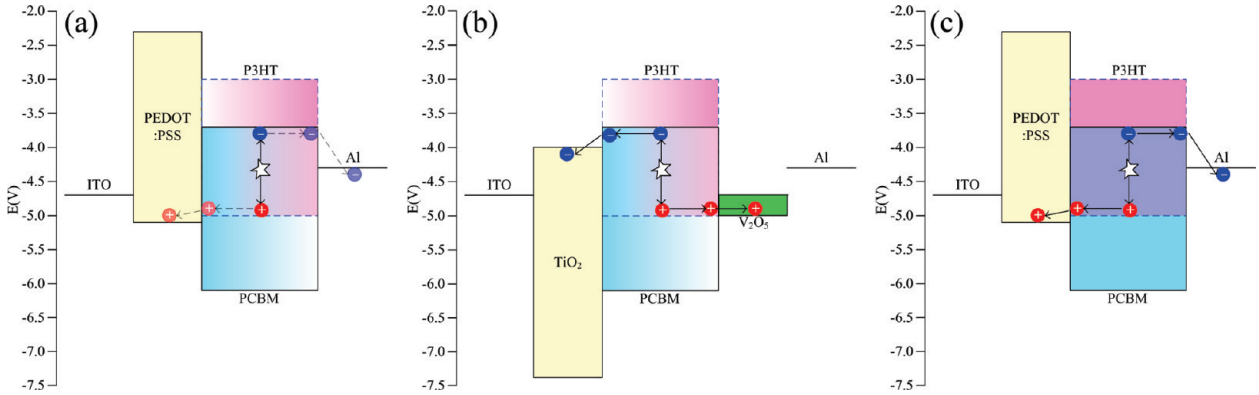

Figure 5. Theoretical energy level diagrams and carrier transportation for the pristine P3HT:PCBM blend in the (a) normal and (b) inverted device architecture, and (c) the annealed P3HT:PCBM blend in the normal device structure. The shading of the color indicates the differences in concentrations.

ning ToF-SIMS depth profiling are similar to those reported previously.[7,18,33] Therefore, this technique is adequate to analyze the nanostructures of organic electronics. It is noteworthy that the iso-intensities of C_2 (PCBM) and S (P3HT) are not entirely complementary. This result is due to the fact that total phase separation did not occur, and therefore, materials are mixed to a certain extent in the thin film.[33] In addition, the absolute amount of materials—rather than the relative ratio between the components—is observed using ToF-SIMS. For the P3HT-enriched region, the absolute amount of PCBM is not necessarily lower than average due to the nanoporous nature of the P3HT polymer. As a result, the distribution of PCBM and P3HT is random and is not complementary.

In the ToF-SIMS patterns and profiles presented in Figures 3a and a, it is clear that the vertical phase separation is suppressed after annealing. The reconstructed 3D cross-sectional image of the PCBM distribution (Figure 3b) is rather uniform, while Figure 3c clearly revealed differences in the fragment distribution that directly relates to the molecular distribution along the vertical axis. The deficiency of P3HT near the PEDOT:PSS interface is due to the lower surface energy of P3HT than of PCBM and is consistent with results reported previously.[13] On the other hand, after annealing, the cross-sectional images of PCBM and P3HT are both uniform along the vertical axis. Using the S/C_2 ratio of the annealed specimen (uniform 1:1 wt % of P3HT:PCBM) as a reference, the composition of the pristine blend can be calculated as a function of depth. It is found that, at the outermost 30 nm, the weight ratio of P3HT:PCBM is 1.85:1, and below 70 nm, the weight ratio is 1:1.16.

The difference in the fragment (molecular) distribution along the vertical axis is consistent with that reported by Campoy-Quiles *et al.*[17] using VASE, where the diffusion of PCBM toward the outer interface after annealing is observed when the blend is coated on PEDOT:PSS. However, VASE has limited lateral resolution, so it is not possible to determine the 3D structure. Using ET, van Bavel *et al.*[7] also reported the enrichment of P3HT near the bottom interface. While all of these studies revealed the diffusion of PCBM toward the outer interface, ET shows significant phase segregation in the depth distribution after annealing, while VASE[17] and ToF-SIMS (shown herein) revealed that the initial phase segregation is leveled after annealing. Such a difference may be due to differences in the fabrication processes.

It is clear that the pristine blend has a higher concentration of P3HT and PCBM at the outer and bottom interfaces, respectively, and the standard device (which consists of ITO/PEDOT:PSS/P3HT:PCBM/Al using the pristine blend) has a power conversion efficiency (PCE) of 1.13%.[17] Because the usual configuration uses the bottom ITO/PEDOT:PSS layer as the anode, enrichment of electron acceptor and donor near the anode and cathode, respectively, is discouraged. This kind of device architecture cannot transport holes and electrons effectively because of the lower concentration of P3HT and PCBM near the PEDOT:PSS anode and the Al cathode, respectively (Figure 5a). As a result, the PCE is lowest for this type of device. On the other hand, for the pristine blend, the inverted structure that matches the distribution of electron acceptors and donors is beneficial to the electrode selectivity; in this case, charge carriers have adequate routes of transportation. For example, by using the structure ITO/TiO_2/P3HT:PCBM/V_2O_5/Al (Figure 5b), where TiO_2-coated ITO serves as the cathode and PCBM is segregated at the bottom interface,[28] the PCE is 2.71%.[36] For the annealed blend in a normal device structure, the electrode selectivity is better due to the diffusion of PCBM toward the Al cathode (Figure 5c), and in addition, the crystallinity of P3HT increases. As a result, a PCE of 3.92% is observed.[17] Understanding the nanoscale molecule distributions and selecting appropriate device structures are critical to enhancing the efficiency of organic electronic devices.

The lateral resolution of ToF-SIMS is around 50 nm and is not comparable with TEM, which usually has a lateral resolution of around 1 nm. Nevertheless, the total data acquisition time for completion of the 3D molecule

distribution in the bulk heterojunction layers presented here is well within 2 h (75 min to collect all 15 images, 25 min for sputtering, and almost real-time reconstruction using a standard Java enabled personal computer). On the other hand, ET requires about 2 h to acquire the tilt series between ±70° at 1 min/image and additional time (on the order of hours) for data reconstruction using a specialized, high-performance computer. In other words, the ToF-SIMS-based technique is much faster than other techniques. In addition, although only about 150 nm is profiled in this work, there is no physical limitation to the total analyzable thickness using ion sputtering. It has been demonstrated that multilayered organic electronic devices with all electrodes in their original states can be studied by ion beam sputtering without prior sample preparation.[32] On the other hand, TEM-based techniques require the sample to be transparent to electrons, and therefore, it is necessary to remove other layers from a device[7,18] or to use focused ion beam-based nanomachining[19] to prepare suitable specimen. Therefore, although the lateral resolution of ToF-SIMS is not as good as ET, the technique presented in this work is versatile and high throughput.

CONCLUSIONS

Using a newly constructed field emission, pulsed Bi_3^{2+} primary ion in scanning time-of-flight secondary ion mass spectrometry with *in situ* Cs^+ ion depth profiling, the 3D nanostructures of bulk heterojunction materials are reported. The results are similar to those reported using electron tomography, indicating that the ion beam-based technique presented herein is adequate for analyzing organic electronics. In addition, the technique presented is much faster and has fewer restraints on specimen preparation in comparison with other techniques. The differences between the pristine and annealed specimens were also observed. While the lateral phase separation is similar before and after annealing, the differences in vertical phase separation significantly affect the performance of devices made with different parameters and device architectures.

METHODS

Fabrication of Photoactive Films: The fabrication process is identical to that reported previously.[17] In short, the photoactive films were prepared by spin coating (2000 rpm, 60 s) a chlorobenzene solution (30 mg/mL, 1:1 weight ratio of P3HT:PCBM) onto the poly(ethylene dioxythiophene):polystyrenesulfonate (PEDOT:PSS)-modified ITO surface. The specimen is optionally annealed at 140 °C for 30 min. The final thickness of the active layer was about 150 nm, and the power conversion efficiency is reported to be 1.13 and 3.92% before and after annealing, respectively.[17]

XPS Measurements: The experiments were performed with a PHI 5000 VersaProbe (Chigasaki, Japan) XPS system. A microfocused (25 W, 100 μm) Al Kα X-ray was used, and the takeoff angle of the photoelectron was 45°. A dual-beam charge neutralizer (7 V Ar^+ and 30 V flooding electron beam) was used for charge compensation. The Ar^+ sputter source was operated at 0.2 kV, 300 nA with an incident angle of 45°. The C_{60}^+ ion source was operated at 10 kV, 10 nA with an incident angle of 70°. Both ion beams were simultaneously rastered over an area of 2 mm × 2 mm.

ToF-SIMS Measurements: The experiments were performed with a PHI TRIFT V nanoTOF (Chigasaki, Japan) ToF-SIMS system. The pulsed primary ion source was Bi_3^{2+} and was operated at 25 kV (0.1 nA DC, 2 fA pulsed) with a 5 μm × 5 μm rastering area at an incident angle of 40°. The analyzer collects negatively charged secondary ions from a direction that is normal to the specimen surface. The data acquisition time is 5 min for each image, and a flooding electron beam (10 V) was used for charge compensation. The resulting images are passed through a low-pass filter in Fourier space to remove random noise. The sputtering is done with a Cs^+ ion beam operated at 1 kV and 50 nA with a 200 μm × 200 μm rastering area at an incident angle of 40°. The final image stack was reconstructed to the 3D volume image using ImageJ.

Acknowledgment. The authors acknowledge sponsorship by the Academia Sinica and the Taiwan National Science Council through Grant Numbers 97-2113-M-001-015, 97-2120-M-002-014, 28-2113-M-001-012-MY2, and 98-2120-M-002-005.

Supporting Information Available: Animated 3D-rendered nanostructure, and reconstructed cross-section structure at different slices. This material is available free of charge *via* the Internet at http://pubs.acs.org.

REFERENCES AND NOTES

1. Yu, G.; Gao, J.; Hummelen, J. C.; Wudl, F.; Heeger, A. J. Polymer Photovoltaic Cells: Enhanced Efficiencies *via* a Network of Internal Donor−Acceptor Heterojunctions. *Science* **1995**, *270*, 1789–1791.
2. Takanezawa, K.; Hirota, K.; Wei, Q.-S.; Tajima, K.; Hashimoto, K. Efficient Charge Collection with ZnO Nanorod Array in Hybrid Photovoltaic Devices. *J. Phys. Chem. C* **2007**, *111*, 7218–7223.
3. Dennler, G.; Sariciftci, N. S. Flexible Conjugated Polymer-Based Plastic Solar Cells: From Basics to Applications. *Proc. IEEE* **2005**, *93*, 1429–1439.
4. Coakley, K. M.; McGehee, M. D. Photovoltaic Cells Made from Conjugated Polymers Infiltrated into Mesoporous Titania. *Appl. Phys. Lett.* **2003**, *83*, 3380–3382.
5. Zhang, F. L.; Jespersen, K. G.; Bjorstrom, C.; Svensson, M.; Andersson, M. R.; Sundstrom, V.; Magnusson, K.; Moons, E.; Yartsev, A.; Inganas, O. Influence of Solvent Mixing on the Morphology and Performance of Solar Cells Based on Polyfluorene Copolymer/Fullerene Blends. *Adv. Funct. Mater.* **2006**, *16*, 667–674.
6. Yang, X.; Loos, J. Toward High-Performance Polymer Solar Cells: The Importance of Morphology Control. *Macromolecules* **2007**, *40*, 1353–1362.
7. van Bavel, S. S.; Sourty, E.; de With, G.; Loos, J. Three-Dimensional Nanoscale Organization of Bulk Heterojunction Polymer Solar Cells. *Nano Lett.* **2009**, *9*, 507–513.
8. Li, G.; Shrotriya, V.; Huang, J. S.; Yao, Y.; Moriarty, T.; Emery, K.; Yang, Y. High-Efficiency Solution Processable Polymer Photovoltaic Cells by Self-Organization of Polymer Blends. *Nat. Mater.* **2005**, *4*, 864–868.
9. Li, G.; Shrotriya, V.; Yao, Y.; Huang, J. S.; Yang, Y. Manipulating Regioregular Poly(3-hexylthiophene):[6,6]-Phenyl-C-61-Butyric Acid Methyl Ester Blends—Route towards High Efficiency Polymer Solar Cells. *J. Mater. Chem.* **2007**, *17*, 3126–3140.
10. Li, G.; Yao, Y.; Yang, H.; Shrotriya, V.; Yang, G.; Yang, Y. "Solvent Annealing" Effect in Polymer Solar Cells Based on Poly(3-hexylthiophene) and Methanofullerenes. *Adv. Funct. Mater.* **2007**, *17*, 1636–1644.
11. Ma, W. L.; Yang, C. Y.; Gong, X.; Lee, K.; Heeger, A. J.

Thermally Stable, Efficient Polymer Solar Cells with Nanoscale Control of the Interpenetrating Network Morphology. *Adv. Funct. Mater.* **2005**, *15*, 1617–1622.
12. Bull, T. A.; Pingree, L. S. C.; Jenekhe, S. A.; Ginger, D. S.; Luscombe, C. K. The Role of Mesoscopic PCBM Crystallites in Solvent Vapor Annealed Copolymer Solar Cells. *ACS Nano* **2009**, *3*, 627–636.
13. Xu, Z.; Chen, L. M.; Yang, G. W.; Huang, C. H.; Hou, J. H.; Wu, Y.; Li, G.; Hsu, C. S.; Yang, Y. Vertical Phase Separation in Poly(3-hexylthiophene): Fullerene Derivative Blends and Its Advantage for Inverted Structure Solar Cells. *Adv. Funct. Mater.* **2009**, *19*, 1227–1234.
14. Palermo, V.; Ridolfi, G.; Talarico, A. M.; Favaretto, L.; Barbarella, G.; Camaioni, N.; Samori, P. A Kelvin Probe Force Microscopy Study of the Photogeneration of Surface Charges in All-Thiophene Photovoltaic Blends. *Adv. Funct. Mater.* **2007**, *17*, 472–478.
15. Hoppe, H.; Glatzel, T.; Niggemann, M.; Hinsch, A.; Lux-Steiner, M. C.; Sariciftci, N. S. Kelvin Probe Force Microscopy Study on Conjugated Polymer/Fullerene Bulk Heterojunction Organic Solar Cells. *Nano Lett.* **2005**, *5*, 269–274.
16. Chiesa, M.; Burgi, L.; Kim, J. S.; Shikler, R.; Friend, R. H.; Sirringhaus, H. Correlation between Surface Photovoltage and Blend Morphology in Polyfluorene-Based Photodiodes. *Nano Lett.* **2005**, *5*, 559–563.
17. Campoy-Quiles, M.; Ferenczi, T.; Agostinelli, T.; Etchegoin, P. G.; Kim, Y.; Anthopoulos, T. D.; Stavrinou, P. N.; Bradley, D. D. C.; Nelson, J. Morphology Evolution *via* Self-Organization and Lateral and Vertical Diffusion in Polymer: Fullerene Solar Cell Blends. *Nat. Mater.* **2008**, *7*, 158–164.
18. Andersson, B. V.; Herland, A.; Masich, S.; Ingans, O. Imaging of the 3D Nanostructure of a Polymer Solar Cell by Electron Tomography. *Nano Lett.* **2009**, *9*, 853–855.
19. Moon, J. S.; Lee, J. K.; Cho, S.; Byun, J.; Heeger, A. J. "Columnlike" Structure of the Cross-Sectional Morphology of Bulk Heterojunction Materials. *Nano Lett.* **2009**, *9*, 230–234.
20. Arslan, I.; Tong, J. R.; Midgley, P. A. Reducing the Missing Wedge: High-Resolution Dual Axis Tomography of Inorganic Materials. *Ultramicroscopy* **2006**, *106*, 994–1000.
21. Parry, S.; Winograd, N. High-Resolution TOF-SIMS Imaging of Eukaryotic Cells Preserved in a Trehalose Matrix. *Anal. Chem.* **2005**, *77*, 7950–7957.
22. Wucher, A.; Cheng, J.; Winograd, N. Protocols for Three-Dimensional Molecular Imaging Using Mass Spectrometry. *Anal. Chem.* **2007**, *79*, 5529–5539.
23. Ostrowski, S. G.; Kurczy, M. E.; Roddy, T. P.; Winograd, N.; Ewing, A. G. Secondary Ion MS Imaging To Relatively Quantify Cholesterol in the Membranes of Individual Cells from Differentially Treated Populations. *Anal. Chem.* **2007**, *79*, 3554–3560.
24. Ostrowski, S. G.; Szakal, C.; Kozole, J.; Roddy, T. P.; Xu, J.; Ewing, A. G.; Winograd, N. Secondary Ion MS Imaging of Lipids in Picoliter Vials with a Buckminsterfullerene Ion Source. *Anal. Chem.* **2005**, *77*, 6190–6196.
25. Fisher, G. L.; Belu, A. M.; Mahoney, C. M.; Wormuth, K.; Sanada, N. Three-Dimensional Time-of-Flight Secondary Ion Mass Spectrometry Imaging of a Pharmaceutical in a Coronary Stent Coating as a Function of Elution Time. *Anal. Chem.* **2009**, *81*, 9930–9940.
26. Lin, Y.-C.; Chen, Y.-Y.; Yu, B.-Y.; Lin, W.-C.; Kuo, C.-H.; Shyue, J.-J. Sputter-Induced Chemical Transformation in Oxoanions by Combination of C_{60}^+ and Ar^+ Ion Beams Analyzed with X-ray Photoelectron Spectrometry. *Analyst* **2009**, *134*, 945–951.
27. Chen, Y.-Y.; Yu, B.-Y.; Wang, W.-B.; Hsu, M.-F.; Lin, W.-C.; Lin, Y.-C.; Jou, J.-H.; Shyue, J.-J. XPS Depth Profiling of Organic Thin Films Using C60 Sputtering. *Anal. Chem.* **2008**, *80*, 501–505.
28. Yu, B.-Y.; Chen, Y.-Y.; Wang, W.-B.; Hsu, M.-F.; Tsai, S.-P.; Lin, W.-C.; Lin, Y.-C.; Jou, J.-H.; Chu, C.-W.; Shyue, J.-J. Depth Profiling of Organic Films with X-ray Photoelectron Spectroscopy Using C_{60}^+ and Ar^+ Co-Sputtering. *Anal. Chem.* **2008**, *80*, 3412–3415.
29. Yu, B.-Y.; Chen, Y.-Y.; Lin, W.-C.; Lin, Y.-C.; Shyue, J.-J. Sputter Damage in Si(001) Surface by Combination of C_{60}^+ and Ar^+ Ion Beams. *Appl. Surf. Sci.* **2008**, *255*, 2490–2493.
30. Cheng, J.; Wucher, A.; Winograd, N. Molecular Depth Profiling with Cluster Ion Beams. *J. Phys. Chem. B* **2006**, *110*, 8329–8336.
31. Lin, W.-C.; Lin, Y.-C.; Wang, W.-B.; Yu, B.-Y.; Iida, S.-i.; Tozu, M.; Hsu, M.-F.; Jou, J.-H.; Shyue, J.-J. Effect of Fabrication Process on the Microstructure and the Efficiency of Organic Light Emitting Diode. *Org. Electron.* **2009**, *10*, 459–464.
32. Lin, W.-C.; Wang, W.-B.; Lin, Y.-C.; Yu, B.-Y.; Chen, Y.-Y.; Hsu, M.-F.; Jou, J.-H.; Shyue, J.-J. Electron Migration of Small Molecules during the Degradation of Organic Light-Emitting Diodes. *Org. Electron.* **2009**, *10*, 581–586.
33. Yu, B.-Y.; Lin, W.-C.; Huang, J.-H.; Chu, C.-W.; Lin, Y.-C.; Kuo, C.-H.; Lee, S.-H.; Wong, K.-T.; Ho, K.-C.; Shyue, J.-J. Three-Dimensional Nanoscale Imaging of Polymer Bulk-Heterojunction Materials by Scanning Electrical Potential Microscopy and C_{60}^+ Cluster Ion Slicing. *Anal. Chem.* **2009**, *81*, 8936–8941.
34. Lin, Y. Y.; Chu, T. H.; Li, S. S.; Chuang, C. H.; Chang, C. H.; Su, W. F.; Chang, C. P.; Chu, M. W.; Chen, C. W. Interfacial Nanostructuring on the Performance of Polymer/TiO_2 Nanorod Bulk Heterojunction Solar Cells. *J. Am. Chem. Soc.* **2009**, *131*, 3644–3649.
35. Zhu, Z. H.; Nachimuthu, P.; Lea, A. S. Molecular Depth Profiling of Sucrose Films: A Comparative Study of C_{60}^{n+} Ions and Traditional Cs^+ and O_2^+ Ions. *Anal. Chem.* **2009**, *81*, 8272–8279.
36. Yu, B.-Y.; Tsai, A.; Tsai, S.-P.; Wong, K.-T.; Yang, Y.; Chu, C.-W.; Shyue, J.-J. Efficient Inverted Solar Cells Using TiO_2 Nanotube Arrays. *Nanotechnology* **2008**, *19*, 255202.